frontiers | Frontiers in Materials

TYPE Original Research
PUBLISHED 25 July 2024
DOI 10.3389/fmats.2024.1427541

OPEN ACCESS

EDITED BY
João Reis,
Fluminense Federal University, Brazil

REVIEWED BY
Michelle Leali Costa,
São Paulo State University, Brazil
Santosh Kumar Sahu,
VIT-AP University, India
Hiasmim Rohem Gualberto,
Instituto Federal Fluminense, Brazil
Jeyanthi Subramanian,
VIT University, India
Fan Zhang,
East China Jiaotong University, China

*CORRESPONDENCE
Dong-Won Jung,
jdwcheju@jejunu.ac.kr

RECEIVED 03 May 2024
ACCEPTED 21 June 2024
PUBLISHED 25 July 2024

CITATION
Haider I, Gul IH, Aziz S, Faraz MI, Khan MA, Jaffery SHI and Jung D-W (2024), Environmental aging of reinforced polymer composite radome: reliability and performance investigation.
Front. Mater. 11:1427541.
doi: 10.3389/fmats.2024.1427541

Environmental aging of reinforced polymer composite radome: reliability and performance investigation

Imran Haider[1], Iftikhar Hussain Gul[1], Shahid Aziz[2,3], Muhammad Iftikhar Faraz[4], Muhammad Ali Khan[5,6], Syed Husain Imran Jaffery[5] and Dong-Won Jung[7]*

[1]Thermal Transport Laboratory, Department of Materials Engineering, School of Chemical and Materials Engineering (SCME), National University of Sciences and Technology (NUST), Islamabad, Pakistan, [2]Department of Mechanical Engineering, Jeju National University, Jeju-si, Republic of Korea, [3]Research Institute for Basic Sciences, Jeju National University, Jeju-si, Republic of Korea, [4]Department of Mechanical Engineering, College of Engineering, King Faisal University, Al-Ahsa, Saudi Arabia, [5]School of Mechanical and Manufacturing Engineering (SMME), National University of Sciences and Technology (NUST), Islamabad, Pakistan, [6]Department of Mechanical Engineering, College of Electrical and Mechanical Engineering (CEME), National University of Sciences and Technology (NUST), Islamabad, Pakistan, [7]Faculty of Applied Energy System, Major of Mechanical Engineering, Jeju National University, Jeju-si, Republic of Korea

In high-speed microelectronic communication, efficient and reliable radome-enclosed antenna performance is highly desired, which depends on consistent dielectric, mechanical properties, and low moisture absorption. The purpose of this study is to investigate the dielectric properties of fiber-polymer matrix composite (PMC) radome over wideband frequency and the impact of environmental aging on its performance. The dielectric constant (ε_r) of the SF/$E_{0.8}$ (80% fiber loading) composite radome material decreased to 4% from its original value (3.93), and dielectric loss (δ) was reduced by 11% from 0.035 (2–18 GHz), while SEM morphology indicated fair interface bonding. Employing the Hallberg and Peck model, equivalent aging time (5–25 years), upon accelerated environmental aging, ε_r was increased up to 3.69%, δ to 9.68%, and the moisture uptake in the SF/$E_{0.8}$ composite was increased from 1.13% to 1.67%, while tensile strength was retained up to 90.62% of its original value (147.83 MPa), compression strength up to 93.56% of its original value (388.54 MPa), flexural strength up to 85.44% of its original value (286.77 MPa), and interlaminar shear strength up to 77.66% of its original value (22.03 MPa), respectively. SF/$E_{0.8}$ radome-enclosed antenna gain was decreased to 1%, and the voltage standing wave ratio (VSWR) was increased to 1.04% from their

Abbreviations: SiO_2, silica; SF/$SiO_{2(f)}$, silica fabric; SF/E_x, silica-fiber/epoxy composite; E, epoxy; H, hardener; x, fraction of the silica fabric; min, minute; ε_r, dielectric constant; δ, dielectric loss; VSWR, voltage standing wave ratio; RH, relative humidity; UTS, ultimate tensile strength; ILSS, interlaminar shear strength; AF, acceleration factor; RH_{use}, relative humidity at actual use condition; RH_{stress}, relative humidity at stress or accelerated conditions, T_{use}, temperature at actual use condition; T_{stress}, temperature at stress or accelerated conditions, Ea, activation energy; eV, electron volt; VSWR, voltage standing wave ratio; $_V$, virgin or unaged; $_A$, aged; T, transverse direction; UCS, ultimate tensile strength; FS, bend strength.

original values. This gradual and small deviation of SF/E_x composite properties and radome electrical performance over the extended aging time is referred to as reliable and effective for radome applications.

KEYWORDS

wave transparent fiber composite, wideband frequency, dielectric properties, tensile properties, reliability

1 Introduction

Applications of fiber-reinforced polymeric composites in microelectronics include printed circuit boards (PCBs), microwave components for 5G communication, and radomes for radars (Kozakoff, 2010). Radomes are exposed to harsh environments while protecting the enclosed antennas (Clarricoats et al., 1982). In high-speed communication where signal transmission is critical, their reliable performance and durability is critically important (Salazar-Cerreno et al., 2022). Polymeric composites (PMCs) with low dielectric constants (<4) are termed wave transparent composites and are suitable for making radomes (Fujimoto et al., 2002). They offer minimum electro-magnetic (EM) signal loss or attenuation, fair mechanical strength, thermal stability, and low moisture absorption (Zhou et al., 2020). However, several challenges for wave-transparent polymeric composites include dielectric instability at different frequencies, high ε_r, higher losses, lower mechanical integrity, and thermal stability at higher working temperatures (Nelo et al., 2019). By introducing fiber-reinforced dielectric polymer composite, ceramics, tunable dielectric materials, frequency-selective surfaces, metamaterial, filler doping, surface modification, functionalization, using hybridcomposites, nanomaterials (Kumar Sahu et al., 2018), 3D materials, upgrading existing material and using low-cost alternative materials with comparable performance (Nair and Jha, 2009) can address future challenges. Sometimes, relatively low working temperatures and the dielectric instability of polymeric composites limit their use (Fu et al., 2019).

Compared to traditional materials, recently, polymers have grabbed excellent responses in various fields of material science (Kumar Sahu et al., 2018; Li et al., 2022). In addition, polymer nanocomposites with excellent mechanical performance have been increasingly sought after in engineering applications such as biotechnology, aerospace, and automotive (Li et al., 2022). Polymers when reinforced with fibers provide both mechanical and functional properties (Lasenko et al., 2023). The signal transmission is affected by the addition of radome as the incident electromagnetic (EM) wave passes through the radome-enclosed antenna (Xing et al., 2023). The dissimilar (material) nature of the antenna and radome tends to change the path of the EM wave, which

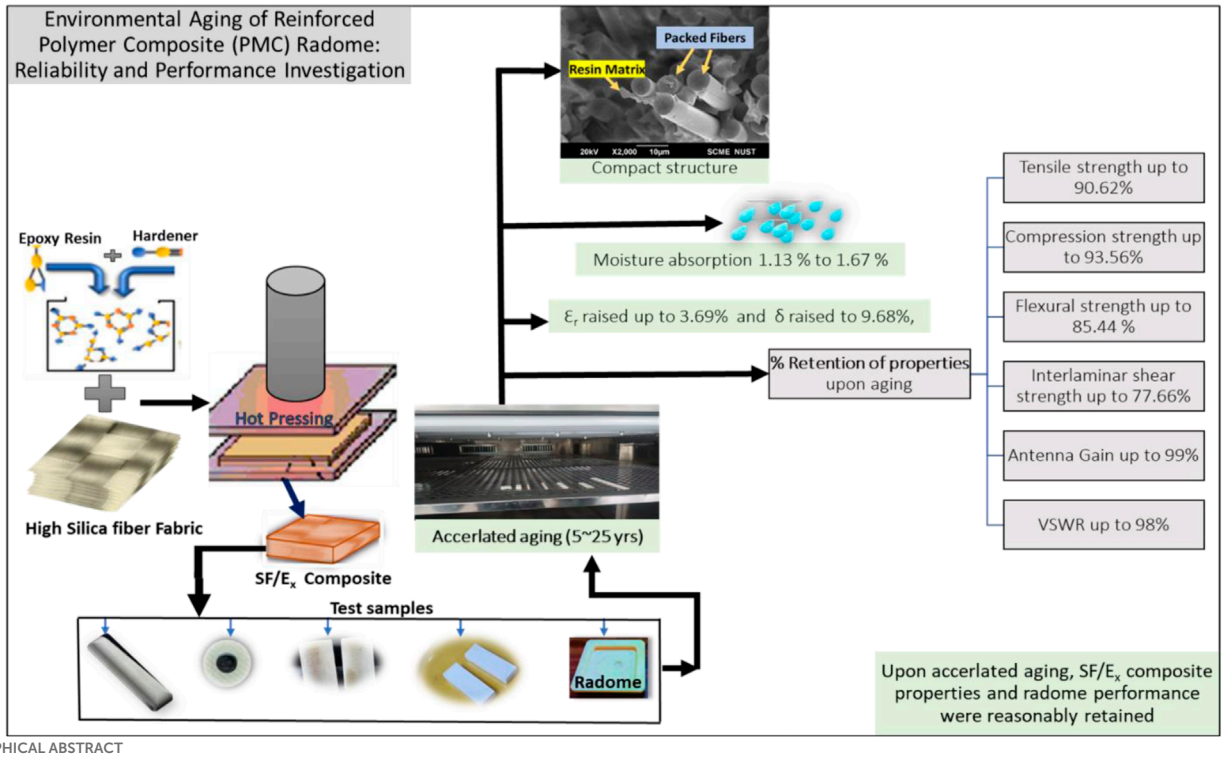

GRAPHICAL ABSTRACT

affects the transmission of signals. So, the radome is desired to be made of such material which provides least hindrance in wave transmission. The unstable and inconsistent dielectric properties lead to variation in capacitance and impedance over time, degradation of radome characteristics, and ultimately reducing overall performance. Limited literature studies were reported on combining long-term stability, reliability, and performance of PMC radomes at various frequencies and environmental aging (Zhou et al., 2015). Upon environmental aging, changes in dielectric characteristics directly and significantly restrict the performance of radome-enclosed antennas through resistance-capacitance (RC) delay and crosstalk noises (Qamar et al., 2020). Fast signal transmission response requires low dielectric constant (ε_r) and low dielectric loss (δ) to reduce RC delay and eliminate crosstalk noises. Eqs 1, 2 indicate the relationship between the signal delay time and the resultant losses (Li et al., 2019), where ε_r is the relative permittivity, c is the speed of light, l is the transmission distance, and t_d is the signal delay time. In Eq. 2, D represents the loss value, a is the constant dependent on the type of losses, f is the frequency, and tan δ is the dielectric loss tangent.

$$t_d = \frac{l + \sqrt{\varepsilon_r}}{c}, \tag{1}$$

$$D = a \times f \times tan\,\delta. \tag{2}$$

The signal transmission process and radome–antenna interactions are shown in Figures 1A, B, where the incident electromagnetic (EM) wave is passing through the radome-enclosed antenna. The slight deviation of the incident EM wave path (1-c) is due to the addition of radome losses. The dielectric instability of reinforced PMC radomes means that either they are unreliable or offer low performance due to variations in their ε and δ (Lasenko et al., 2023). The reliability and sustainable performance of the radome require these properties to remain intact for a longer duration (Choi et al., 2012). Wave-transparent fiber-reinforced PMCs with frequency-stable dielectric properties (Haider et al., 2023a), mechanical integrity (Lasenko et al., 2023), thermal stability (Haider et al., 2023b), and low moisture uptake (Wang et al., 2021) offer balanced EM properties and structural integrity (Rafieipour et al., 2021). The good performance, strong thermal conductivity, lower thermal expansion, and nominal cost of glass fiber make it prospective for use in radome applications (Gu et al., 2024). The minimal variation in ε and δ can be referred as dielectric stability (Fu et al., 2019). Dielectric properties of PMCs may change with frequency and upon environmental aging (Park et al., 2019). Aging itself is a slow process in which the material properties deteriorate over time due to UV radiation, temperature, moisture, mechanical dust, inside physical cracking, and/or a combination of these stresses (Jawaid et al., 2016). Consistent and stable properties for these PMCs, especially against environmental aging, still needed to be explored (Islam et al., 2023).

The service life of fiber-reinforced composites is usually measured in years (Maxwell et al., 2005). Given the fact that reinforced plastics are viscoelastic materials, their properties are strongly time- and temperature-dependent. Nevertheless, a swift, feasible, and suitable method to study the variations is possible by inducing accelerated aging conditions (Hallberg and Peck, 1991). Evaluation of the actual change in their properties may require several years (Khattak et al., 2018). For optimized performance (Champa-Bujaico et al., 2024), to predict and estimate the long-term performance of composites, the Arrhenius model can correlate accelerated aging with natural aging (Panaitescu et al., 2019). The rate of degradation is accelerated with the increase in temperature, as shown by Eq. 3.

$$k = \mathrm{A}\exp\left(\frac{-\mathrm{Ea}}{RT}\right) \text{ or } \ln k = \ln \mathrm{A} + \frac{-\mathrm{Ea}}{RT}, \tag{3}$$

where k is the degradation rate (1/time), A is the constant of the material and degradation process, E_a is the activation energy, R is the universal gas constant, and T is the temperature in Kelvin (K), which is a dominant factor of acceleration in the aging process. The logarithm of 1/k is the time for a material property to degrade to a certain value, with the slope Ea/R (Silva et al., 2014). Furthermore, over prolonged environmental exposure (time, temperature, and % RH), the operational life, reliability, and durability of reinforced PMCs vary, which needs to be determined (Wang et al., 2020). To study the impact of these stresses in a suitable way, derived from the Arrhenius law, the combined effect of temperature and humidity is described by Eq. 4, which is known as the Hallberg and Peck model (Hallberg and Peck, 1991).

$$AF = \left(\mathrm{RH}_{\mathrm{stress}} - \mathrm{RH}_{\mathrm{use}}\right)^3 * exp\left[\frac{Ea}{K\left(\frac{1}{Tuse} - \frac{1}{Tstress}\right)}\right], \tag{4}$$

where AF is the acceleration factor, RH_{stress} is the relative humidity at stress or accelerated conditions, RH_{use} is the relative humidity at the actual use condition, T_{use} is the temperature of use condition, and T_{stress} is the temperature stress or accelerated conditions stress. In recent years, silica fiber–epoxy wave-transparent composites (Tang et al., 2021) have been investigated due to their dielectric and mechanical properties and durability (Silva et al., 2014).

Aging is a very slow process in which material properties deteriorate with time and it cannot be stopped. However, impact aging can be reduced by the adoption of proper mitigation strategies (McKenna, 2012). A very long time, i.e., several years, is required to obtain the actual effects of aging on radome's structural properties, and sometimes, due to uneasy and inaccessible locations, radome maintenance, repair, and quality inspection, it is not easily manageable (Park et al., 2019). Aging-related deteriorations can be studied by simulation and modeling. Temnikov et al. used different correlations for service life prediction to avoid any earlier failures (Liu et al., 2023). Keeping this research gap, there is a need to study the high-silica fiber/epoxy composite dielectric properties (ε_r and δ) upon accelerated environmental aging (McKenna, 2011; Rodriguez, 2017; Starkova et al., 2022). Polymer-based composites have attained significant attention due to their easy fabrication (Amirapu et al., 2022). Based on Eq. 4, current work investigates the effect of aging conditions on the properties of reinforced wave-transparent composite radomes. Appropriate fractions of high-silica fiber–epoxy composite samples were fabricated. The impact of environmental aging on the reliability of radome/samples was analyzed by establishing accelerated aging conditions equivalent to 5–25 years of aging. Dielectric constant,

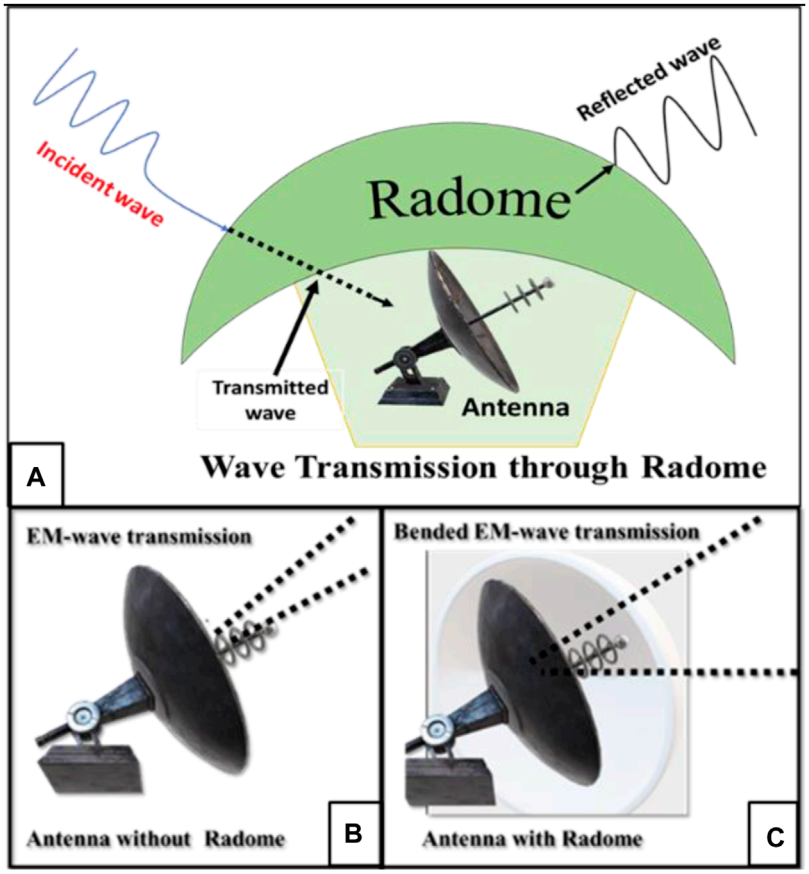

FIGURE 1
Radome–antenna interaction. **(A)** Wave transmission process, **(B)** Antenna with Radome, **(C)** Antenna without Radome.

dielectric loss, moisture absorption, and mechanical and radome properties were examined. It is worth noting that this cost-effective grade of silica glass fibers (Wallenberger, 1999) has not been investigated for radome applications. In addition, the evaluation of changes in properties over long-term aging times is focused on estimating their performance. The current work combinedly assesses the radome property, performance over wide frequency, and impact of aging upon the specified conditions. Environmental aging studies are needed for earlier prediction of the degradation of material properties to contribute to the sustainability and long-term reliability of fiber composites.

2 Materials and methods

2.1 Materials

After comparing various reinforcements and matrices, as mentioned in Table 1, the cost-effective glass fibers named high-silica fiber [$SiO_{2(f)}$] fabric and epoxy resin were used. Unidirectionally woven high-silica glass fiber $SiO_{2(f)}$ (HTSB-026-FW, SiO_2 ≥ 95.63%, fiber dia. ~6.0–10.0 μm, surface density ~2.30 g/m^2, ply thickness = 0.2 mm, softening point ≥1,700°C) was supplied by Mega Tech International, Islamabad, Pakistan. The subscript (f) refers to the fabric. Liquid epoxy resin, Zepoxy RER 128, Bisphenol A epoxy resin (density = 1.10 kg/m^3, μ = 11–13 Pa ∗ s, epoxy equivalent weight 192 g/eq, epoxy content = 22.5%) (procured from RESSICHEM Pvt. Ltd. Karachi, Pakistan), and hardener Zepoxy-REH-140 (amine value = 370–410 mg KOH/g, density = 0.95 kg/m^3, μ = 10–15 Pa ∗ s) were used. Methanol (Sigma-Aldrich ≥99.9%) was used as a diluent in the preparation of the matrix solution, while the commercial grade methanol was used for washing the reinforcement fabric. The relative cost ratio of high-silica glass fiber and epoxy resin is considered as reference "1."

2.2 Composite preparation

Samples of SF/E_x composite radome materials were fabricated with an increasing fraction of $SiO_{2(f)}$ x = 40 to 90 (wt.%) and were identified (SF/$E_{0.4}$, SF/$E_{0.5}$, SF/$E_{0.6}$, SF/$E_{0.7}$, SF/$E_{0.8}$, and SF/$E_{0.9}$). The high-silica glass fiber-$SiO_{2(f)}$ fabric was cut in plies and dried (30 min at 100°C) for moisture removal. The details of experimental conditions are mentioned in Table 2.

Resin matrix was prepared by gentle mixing of two-part epoxy resin (A and B), diluted with methanol, and poured

TABLE 1 Comparison of different reinforcing fibers and resin matrixes.

Fiber	Quartz glass	High-silica glass	BN	D-glass	E-glass
ρ (g/cc)	3.78	3.9	3.5	4	6.13
Tensile modulus (GPa)	72	80	400	52	72
Relative cost ratio	5:1	1:1	4:1	3:1	2:1
Resin	**Cyanate ester**	**Polyimide**	**Epoxy**	**PTFE**	**Phenolic**
ε_r	3.1–3.5	2.6–2.8	3.7–3.9	2.3	6.6–8
Relative cost ratio	6:1	10:1	1:1	4:1	5:1

TABLE 2 Experimental conditions during fabrication.

Fabric drying (°C)	Epoxy resin to hardener	Pressure (bar)	Cure (°C)	Post-cure (°C)
100	(A: B) 1: 0.6	10	8 h @ 120	16 h @ 140

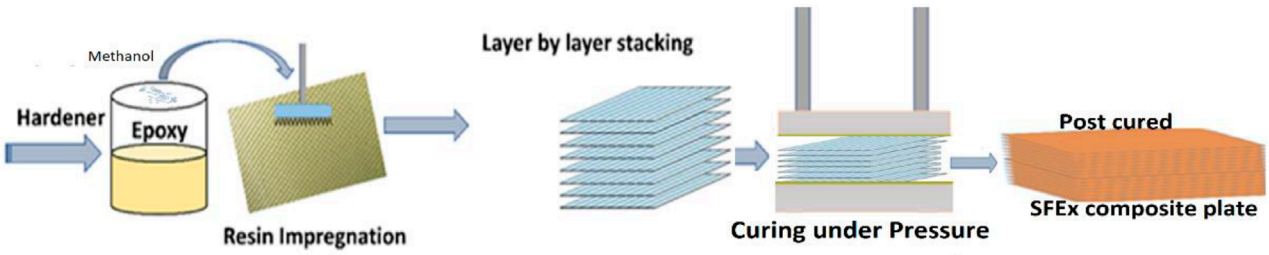

FIGURE 2
SFE composite fabrication scheme.

on fabric sheets. Impregnated sheets were placed in die molds and hot-pressed (10°C/min) to cure, as shown in Figure 2. Then, the laminated composite plate was extracted and post-cured.

2.3 Accelerated environmental aging

Aging deteriorates the material properties slowly, leading to bad performance. Equivalent to 5–25 years of ambient aging, the accelerated aging conditions were estimated using the Hallberg and Peck model (Hallberg and Peck, 1991). The service temperature was taken as 25°C, 40% RH; the accelerated conditions were considered as 95°C, 85% RH; and the activation energy was Ea = 0.8 (Denis et al., 2017). By substituting these values (service and accelerated conditions) in Eq. 4, the accelerated aging time was determined. Figure 3 shows the environmental chamber used in the study. The stress cycling started with a 25-minute ramp-up time in a climate chamber from 25°C, 40% RH (Tmin); to 95°C, 85% RH (Tmin); then a 25-min dwell time at 50°C; and a 25-min ramp-down time.

3 Characterization

The dielectric properties (ε_r and δ) of SF/$E_{0.4}$, SF/$E_{0.5}$, SF/$E_{0.6}$, SF/$E_{0.7}$, SF/$E_{0.8}$, and SF/$E_{0.9}$ composites were measured (2–18 GHz) using a PNA Network Analyzer 8362B (Agilent) instrument. Chemical nature was investigated by Fourier transform infrared spectroscopy (FTIR) (PerkinElmer Spectrum 100, United States), ranging from 4,000 cm^{-1} to 400 cm^{-1}. The moisture absorption of the unaged SF/$E_{0.8}$ composite and those exposed to accelerated aging conditions (0, 5, 10,15, 20, and 25 years) (three samples) in traverse fiber directions was determined (Park et al., 2019). Mechanical properties such as ultimate tensile strength (UTS), ultimate compressive strength (UCS), bending strength, and interlaminar shear strength (ILSS) were determined (Park et al., 2019; Saba et al., 2019) by Universal Testing Machine (UTM, AGX-Plus Shimadzu, Japan) at a test speed of 2 mm/min at 100 KN load. Morphology was determined using the scanning electron microscope (JSM-6490-EOL Japan) at an accelerating voltage of 20 KV. Details are summarized in Table 3, and test samples are shown in Figures 4A–H. In addition, radome characteristics were measured enclosed with patch antenna (SF/$E_{0.8}$).

FIGURE 3
Environmental aging in the climate chamber.

TABLE 3 Summary of characterization.

S. No.	Description	Dimension	Method	No. of samples
1	Dielectric constant	φ 3.5 mm	ASTM D 150	01 each proportion
2	Dielectric loss	φ 3.5 mm	ASTM D 150	01 each proportion
3	Chemical structure	5–7 mg	FTIR	01 each proportion
4	Moisture absorption	10 cm × 10 cm × 10 cm	ASTM D 570	03 ($SF/E_{0.8}$)
5	Tensile strength	250 mm × 25 mm × 2.5 mm	ASTM 3039	03 ($SF/E_{0.8}$)
6	Compressive strength	25.4 mm × 12.7 mm	ASTM 6641	03 ($SF/E_{0.8}$)
7	Bend strength	36 mm × 12 mm × 6 mm	ASTM 7264	03 ($SF/E_{0.8}$)
8	Interlaminar shear strength	36 mm × 12 mm × 6 mm	ASTM D 2344	03 ($SF/E_{0.8}$)
9	Morphology	5 mm × 5 mm × 2 mm	SEM	01 ($SF/E_{0.8}$)

4 Results and discussion

4.1 Fourier transmission infrared (FTIR) spectroscopy

FTIR spectra recorded from 4,000 to 400 cm^{-1} showed the presence of organic and inorganic networks in the fiber-reinforced-epoxy (SF/E) composites, as shown in Figure 5. The FTIR spectrum (x = 40–90) exhibited similar higher region bands as -OH stretching reflected the hydroxyl linkage found at 3,440 cm^{-1} and 2,922.5 cm^{-1}, whereas the vibration peak at 1,639.6 cm^{-1} showed the C=O double bond of carbonyl complexes similarly reported (Adekomaya et al., 2018). The dehydration reaction formed the secondary alcohol and aromatic ether groups, which were then oxidized to carbonyl complexes observed by the vibration peak at 1,643 cm^{-1} corresponding to the C=O double bond. The peak at 1,178.1 cm^{-1} showed the C–N–C stretching of tertiary amine, and the absorption peak at 1,096 cm^{-1} was attributed to C–O–C stretching; however, the expansion vibration peak at 800.5 cm^{-1} attributed C–H linkages, and Si–O–Si deformation was observed at 466 cm^{-1}, as previously studied (Cecen et al., 2008). The identical FTIR spectrum is in agreement with the typical glass fiber/epoxy resin composite (Rodriguez, 2017), irrespective of fiber content, as a result of the crosslinking of epoxy/amine upon curing (Chen et al., 2021). The reinforcing fibers improve the structural stability of epoxy resin and thermal properties of the composite (Pradhan et al., 2022).

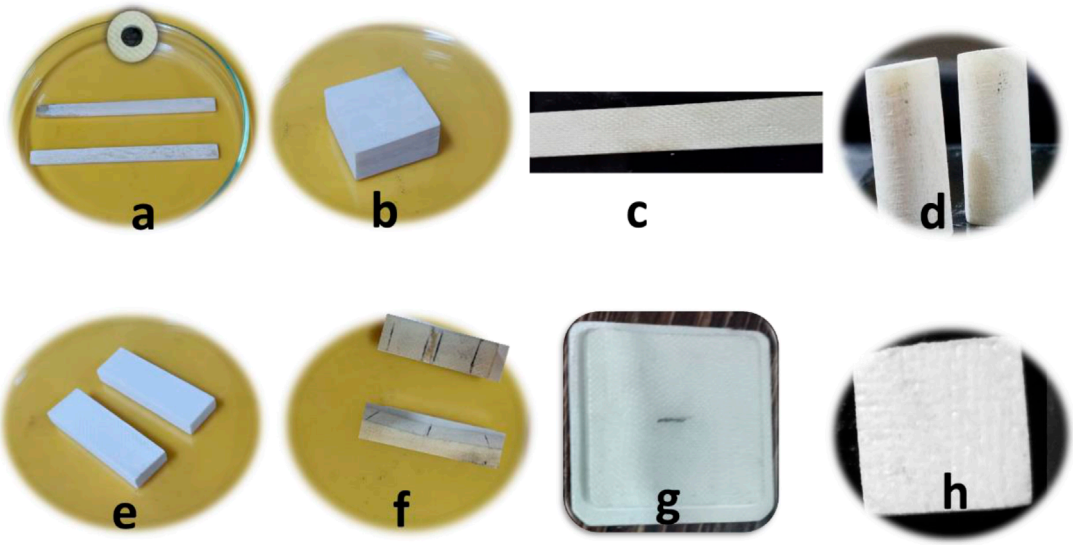

FIGURE 4
SF/E_x composite: **(A)** ε_r and δ test sample, **(B)** moisture test sample, **(C)** tensile strength test sample, **(D)** compression test sample, **(E)** ILSS test sample, **(F)** Bend test sample, **(G)** radome, and **(H)** morphology test sample.

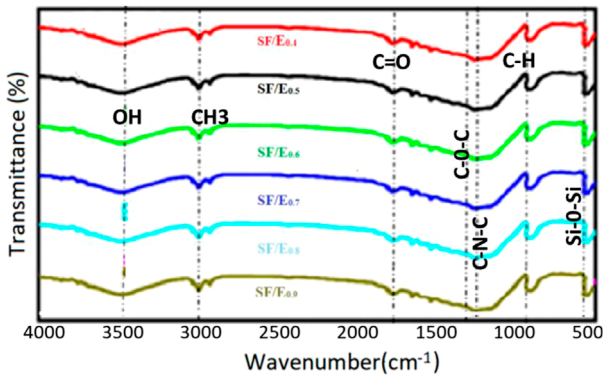

FIGURE 5
FTIR spectra of the SF/E (x = 0.4–0.8) composite radome material.

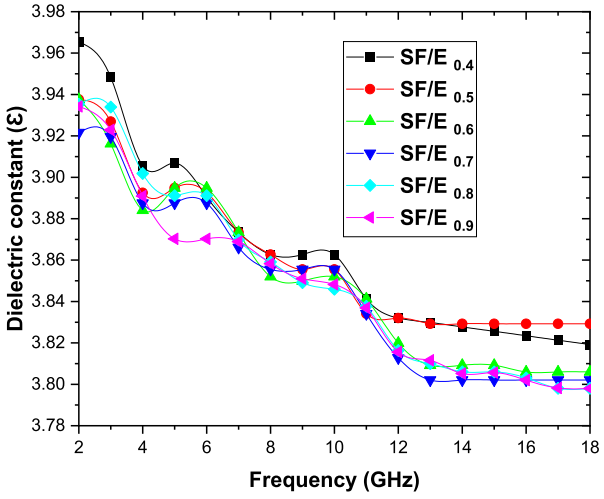

FIGURE 6
Dielectric constant of the SF/E (x = 0.4 to 0.8) composite radome material.

4.2 Dielectric properties

In this study, the variation in dielectric properties (ε_r and δ) of the fabricated SF/Ex composite was evaluated over a wideband frequency. Figures 6, 7 show the ε_r and δ values of SF/$E_{0.4}$, SF/$E_{0.5}$, SF/$E_{0.6}$, SF/$E_{0.7}$, SF/$E_{0.8}$, and SF/$E_{0.9}$ over a wideband frequency.

ε_r of SF/$E_{0.4}$ was reduced from 3.96 to 3.81 (3.78%), SF/$E_{0.5}$ was reduced from 3.93 to 3.82 (2.79%), SF/$E_{0.6}$ was reduced from 3.93 to 3.80 (3.30%), SF/$E_{0.7}$ was reduced from 3.92 to 3.80 (3.06%), SF/$E_{0.8}$ was reduced from 3.93 to 3.79 (3.31%), and SF/$E_{0.9}$ was reduced from 3.93 to 3.80 (3.30%). With the increasing frequency, ε_r decreased due to a reduction in the space-charge polarization effect. At higher frequencies (11–18 GHz), the polarization mechanism showed no response, which resulted in a further decrease in ε_r from initial values. Moreover, from 11 GHz up to 18 GHz, when compared among all the proportions, a minimum variation in the dielectric constant of SF/$E_{0.8}$, referred to its stability in the dielectric constant value. The decrease in the values of the dielectric constant revealed the smooth propagation of the signal through the reinforced composite radome material. The δ value of SF/$E_{0.4}$ was 0.036, SF/$E_{0.5}$ was 0.035, SF/$E_{0.6}$ was 0.035, SF/$E_{0.7}$ was 0.032, SF/$E_{0.8}$ 0.031, and SF/$E_{0.9}$ was 0.031 (13.8% lower from the initial value), as shown in Figure 7. Likewise, ε_r and δ values were also decreased with the increasing silica fiber ratio in the reinforced composite (Haider et al., 2023b). Increasing silica fiber up to 70% (SF/$E_{0.7}$) variation in δ was found to be approximately 3%, but with further fiber loading up to 80%, no significant variation was observed. For this ratio (SF/$E_{0.8}$), it is attributed that δ became constant or

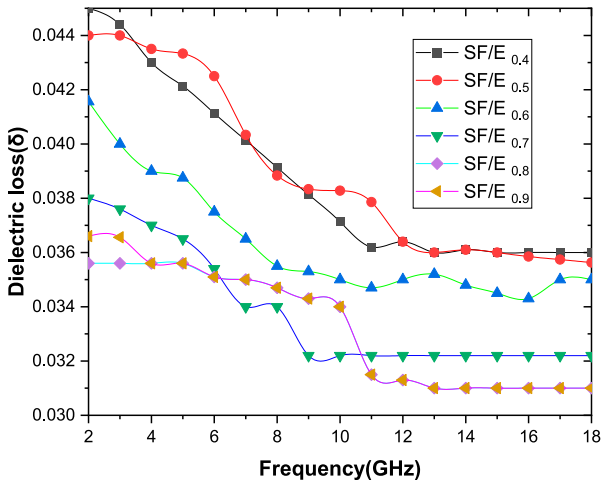

FIGURE 7
Dielectric loss (δ) of the SF/E (x = 0.4–0.8) composite radome material.

TABLE 4 Radome–antenna performance.

Frequency (2–18 GHz)	Gain	VSWR
	dB	
Without radome	10.31 to 10.56	1.44 to 1.29
With $SF/E_{0.8}$ composite	7.67 to 7.33	1.47 to 1.66

stable without remarkable variation. Reduction in δ decreases the parasitic capacitance and signal delay time which can improve the signal transmission quality. The dropping of δ was observed with the increasing silica fiber ratio to 80%, and it became persistent (δ = 0.031) even upon adding more silica fiber (up to 90%). It is referred to as a higher wave transparency of the $SF/E_{0.8}$ composite for speedy signal transmission. No notable change was observed in ε_r and δ ($SF/E_{0.8}$) even after increasing fiber loading up to 90% $SF/E_{0.8}$. The low ε_r and δ values of the $SF/E_{0.8}$ composite lowered polarization and decreased the charge migration process (Bilaç and Duran, 2023) within the composite, which is referred to as fair dielectric stability as well.

From the radome-enclosed antenna results, the addition of the $SF/E_{0.8}$ composite radome has contributed to add-on the losses by reducing the antenna gain and VSWR, as shown in Table 4. The key motive for using radomes is antenna protection without minimally interfering with its performance. This addition of losses was due to the difference in the material nature of the $SF/E_{0.8}$ composite and antenna, where the antenna gain was reduced by 2.6 dB by the addition of the composite radome. It revealed that the signal transmission ability of the antenna has been reduced as the radiated power delivered to the antenna from its transmitter was reduced. When comparing the variation in the gain value over the entire wideband frequency, it was noteworthy that the gain was slightly increased at a higher frequency, which means the efficiency of the antenna has been minimally affected (Hong et al., 2020). It was due to the decrease in ε_r and δ, which decreased the parasitic capacitance and signal delay time, which, in turn, resulted in improved signal transmission.

4.3 SEM morphology

Figures 8A–D display the SEM images of the reinforced composite $SF/E_{0.8}$, where fiber-to-resin adhesion can be seen along with an excellent arrangement of high-silica fibers in the resin matrix. During sample preparation, imbalanced tooling can put shear stresses on the composite surface (Siddique et al., 2023). The fabric layer-to-layer (Figures 8A, B) and fabric–resin interfaces indicated the uniform distribution of resin on fibers. The compact composite structure showed strong interfacial bonding, which can be effective against environmental aging. However, the few weak zones, including voids, were also there and might be susceptible to aging impacts where more chances of fiber–resin debonding were reported. One of the failure cases of glass fiber composites reported (Deng et al., 2022) is related to poor interfacial bonding. However, from these SEM images, this packed structure is responsible for stable structural and mechanical properties, as reported by Fu et al. (2019). The interface region controls the stress transfer between the fiber and resin matrix (Karger-Kocsis et al., 2015), with appropriate interfacial properties, which directly contribute toward the durability, optimum performance, and reliability of glass fiber composites. The sustainable machining of the composite implies a finished surface and improved structural stability (Ahmad et al., 2024).

4.4 Moisture absorption upon aging

The determination of moisture absorption is of key importance during environmental aging as the higher dielectric constant of water (ε_r = 70) can directly and adversely affect the dielectric performance and wave transmission through the composite radome (Cormier and Joncas, 2010). In reinforced composites, the traverse (T) fiber direction is more susceptible to absorbing moisture than the longitudinal fiber direction (Boukhoulda et al., 2006). The average moisture absorbed was 1.13% (unaged), 1.29% (5 years), 1.45% (10 years), 1.51% (15 years), 1.58% (20 years), and 1.67% (25 years). Upon accelerated aging, moisture absorption gradually increased from 1.13% to 1.67%, in agreement with the moisture absorption studies of the glass fiber-reinforced composite (Kumosa et al., 2004). The cross section of the exposed surface or the upper layer of composite specimens was affected by the hydroxyl linkage of the water molecule, which tends to reduce the adhesion between the packed interfacial boundaries. The amount of moisture uptake in the $SF/E_{0.8}$ composite increased from 1.13% (at time = 0 years) to a maximum of 1.67% (at time = 25 years). Upon aging, the increased moisture absorption raised ε_r and δ, which possibly resulted in hindrances in signal transmission through a radome-enclosed antenna. However, moisture absorption can be reduced by coating (Khan et al., 2022) the surface of the composite.

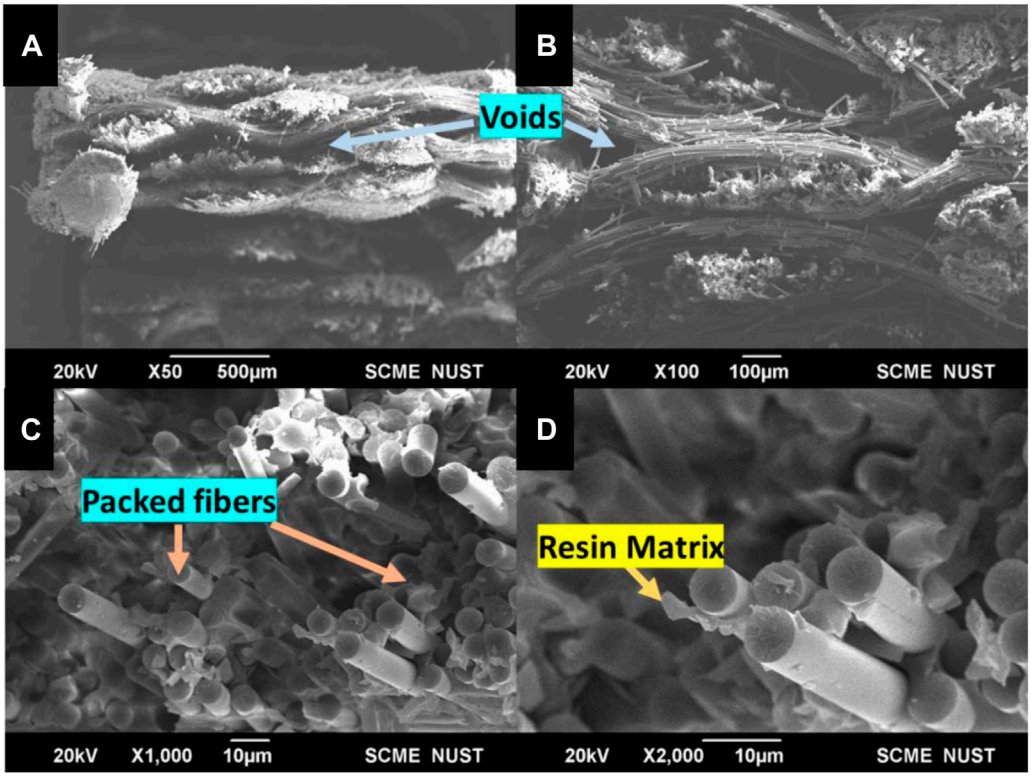

FIGURE 8
Morphology of the SF/$E_{0.8}$ composite radome material depicting **(A)** Voids **(B)** Voids **(C)** Packed fibers **(D)** Resin Matrix.

4.5 Radome properties upon aging

Figures 9, 10 represent the effect of environmental aging on the SF/$E_{0.8}$ composite radome material and PMC radome enclosed with a patch antenna. Figure 9 showed a gradual increase with a moderate variation in $\mathfrak{E}_r$ and δ values. The increased $\mathfrak{E}_r$ value of the antenna substrate increases the chance of polarization with the composite, thus affecting its radiation properties. Figure 10 shows that the antenna gain decreased from 7.67 to 7.59 and VSWR increased from 1.42 to 1.48. At different accelerated aging times, these properties decreased from 5 to 7%, which highlights that microwave parameters were not significantly affected. From these values, the performance of the antenna enclosed with radome was reduced but termed as reliable and efficient in signal transmission. The effect of environmental aging on the SF/$E_{0.8}$ composite radome material and PMC radome enclosed with the patch antenna was evaluated. Upon aging, from 5 years to 25 years, the $\mathfrak{E}_r$ value of SF/$E_{0.8}$ of the unaged composite (3.79) was slightly increased to 0.26% (5 years), 0.79% (10 years), 1.85% (15 years), 3.17% (20 years), and finally to 3.69% (25 years). Similarly, δ was increased from 0.031% to 3.69% (5 years), 4.84% (10 years), 6.77% (15 years), 8.39% (20 years), and 9.68% (25 years). Figure 9 shows that the increase was found gradual with a moderate variation in $\mathfrak{E}_r$ and δ values. The antenna gain decreased from 7.67 to 7.59 and VSWR increased from 1.42 to 1.48. At different accelerated aging times, these properties were decreased from 5% to 7%, which highlights that microwave parameters were not significantly altered. The performance of the antenna enclosed with the radome decreased, although it was reliable and efficient in signal transmission.

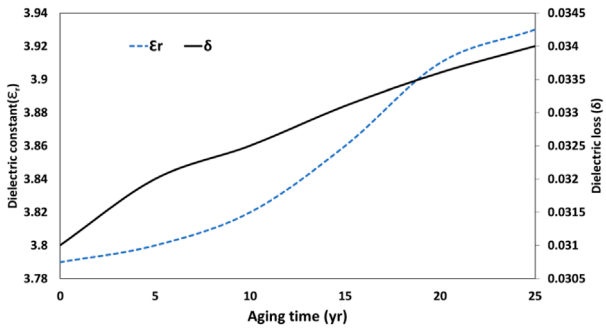

FIGURE 9
SF/$E_{0.8}$ composite radome performance ($\mathfrak{E}_r$ and δ).

The radome–antenna-coupled performance depends on dielectric properties directly, which affects the antenna gain and VSWR (Muneer Ahmed et al., 2024). Figure 10 shows the decreasing trend of the gain and increase in VSWR, meaning that the aging process has increased the dipole mobility and charge polarity, thus amplifying the polarization and charge migration processes. This has reduced the efficiency of the radio frequency power transmission passing through the radome-enclosed antenna. It indicated that more power is reflected than transmitted. Overall,

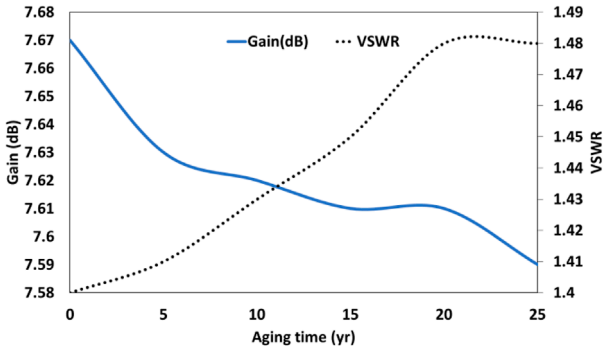

FIGURE 10
SF/$E_{0.8}$ composite radome performance (gain and VSWR).

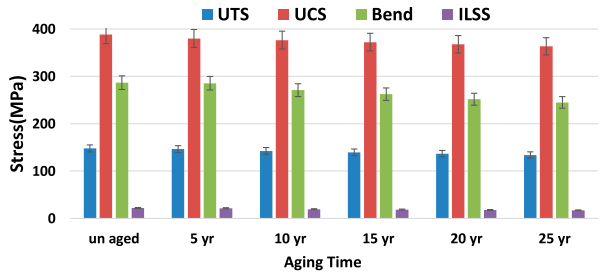

FIGURE 11
Mechanical properties of the SF/$E_{0.8}$ composite radome material upon accelerated aging.

the accelerated aging increased the VSWR to 7% upon 20 years of aging, which means signal delay time is raised, leading to low transmission quality. The decreasing antenna gain and increasing standing wave ratio can lead to a less efficient system. However, in RF communication, the VSWR below 2 is considered reasonable, as mentioned for the performance of radomes in ultra-wide and communication applications (Ha et al., 2022). The VSWR increased upon aging; however, after 22 years, the curve decline of VSWR is negligible at 0.3%–0.4% from its maximum value of 1.48. This marginal decrease is possibly due to the unexpected aging impact, or it might be some measurement. The results of this study provide some clues for radome–antenna-coupled performance upon aging, which can be implemented with the consideration of other contributing factors. For the high-silica fiber/epoxy composite radomes, this slight change or even surface roughness (Khan et al., 2023a) can impact the appropriate performance for longer durations. Nevertheless, the environmental conditions in this study were limited to time, temperature, and humidity. Other environmental aging factors, such as UV, lighting, wind, chemical attack, salty marine environment (Khan et al., 2019), and fatigue, were beyond the scope of this work due to higher variability.

4.6 Mechanical properties upon aging

Figure 11 displays the mechanical properties of the SF/$E_{0.8}$ composite at different aging times (unaged, 5, 10, 15, 20, and 25 years), where the UTS decreased from 147.83 MPa to 133.94 MPa, UCS decreased from 388.54 to 363.51 MPa, flexural strength decreased from 286.77 MPa to 245.02 MPa, and interlaminar shear strength (ILSS) decreased from 22.03 to 17.11 MPa. Initially, the virgin or unaged composite structure was tough and intended to bear a high compressive load which gradually decreased. Environmental aging has weakened the matrix (thermosetting epoxy resin), thus causing a reduction in mechanical properties after every 5 years of aging. The maximum reduction was seen for flexural strength, which was 17.22% in comparison to the reduction behavior of UTS and UCS. The reinforcement (high-silica fibers) was not directly affected, but the composite structure transformed from tough to slightly brittle due to the aging of the organic component (epoxy resin). The interlaminar shear strength (ILSS), which has critical significance in reinforced composites (Sahu and Sreekanth, 2022) where they are subjected to transverse loading, was reduced from 22.03 to 17.11 MPa. The brittle matrix (epoxy resin) that carries interlaminar shear determines the interfacial adhesion of fiber to the matrix, delamination failure, and the quality of fiber-to-matrix bonding. The silica fibers have non-planar interlaminar regions, so they were expected to experience various failures before interlaminar shear failure induced by the machining process (Khan et al., 2023b). The reinforcement ($SiO_{2\ (f)}$) to matrix (epoxy) ratio is a significant factor in multilayer composites where layer-to-layer binding is important for structural integrity. The aging of the SF/$E_{0.8}$ composite resulted in the deterioration of composite interlayer bonding due to the plasticization of thermoset epoxy resin and internal stresses, which degraded mechanical properties gradually without a sharp decrease.

Using Eq. 5, the % property retention was accomplished.

$$\%\,Rp = \left(\frac{Pt}{Po}\right) \times 100, \tag{5}$$

where % R_p is the percentage retention of property, P_t is the property value at (aged) time t, and P_o is the initial property value of the virgin composite. In reference to the virgin SFE composite mechanical property dataset, the % property retention is tabulated in Table 5.

Table 5 simplified the comparison of mechanical properties between the unaged and the aged SFE composite samples. The accelerated environmental exposure resulted in an overall reduction in mechanical properties, but the % retention seems reasonable, given the specified aging conditions under study. The tensile and compressive strength were retained to 90.6% and 93.56%, respectively, to their original values. However, the bending strength and the interlaminar shear strength were found to have a higher reduction but were retained at 85.4% and 77.6%, respectively. The % retention indicated that the SFE composite experienced less influence from tensile and compressive loadings than bending and interlaminar shear forces. In unidirectional composites, the compressive and tensile properties are minimally varied, and the matrix and interface experience higher stresses during bending/interlaminar loading, as likewise reported (Selzer and Friedrich, 1997). The long hot–humid climate is responsible for absorption and desorption, which mainly affected the bending

TABLE 5 Percentage of mechanical property retention upon aging.

Property	UTS (MPa)	Retention	UCS (MPa)	Retention	FS (MPa)	Retention	ILSS (MPa)	Retention
Unaged	147.8	%	388.54	%	286.77	%	22.03	%
5 years	146.3	98.99	380	97.80	285.54	99.57	20.3	92.14
10 years	142.6	96.48	376.6	96.92	270.87	94.45	19.51	88.56
15 years	139.65	94.49	372.34	95.83	262.45	91.51	18.83	85.47
20 years	136.76	92.53	367.76	94.65	251.75	87.78	17.8	80.79
25 years	133.94	90.62	363.54	93.56	245.02	85.44	17.11	77.66

and shearing between the composite layers, leading to interfacial debonding, as indicated previously (Mansouri et al., 2019). The matrix plays the most important role in any polymer composite as it binds to the fiber layer (Nivedhitha et al., 2023). As shown in this work, the epoxy resin matrix is mainly defined by the interface's response or resistance to accelerated aging, which gradually degrades the mechanical properties. Thus, suitable substitute composites with sustainable properties can overcome problems faced by the conventional materials (Nivedhitha and Jeyanthi, 2023).

5 Conclusion

In conclusion, this work has evaluated the dielectric properties of high-silica glass fiber/epoxy SF/E_x composites in a wide frequency band (2–18 GHz). In addition, the impact of environmental aging on structure, moisture absorption, mechanical properties, and morphology was experimentally determined from 5 to 25 years of aging (employing the Hallberg and Peck model). SF/$E_{0.8}$ reinforced the composite radome. The variation in properties upon accelerated aging was experimentally validated and quantified.

- Increasing silica fibers, the SF/$E_{0.8}$ composite exhibited ε_r and δ from ε_r = 3.93 to 3.79 and δ = 0.035 to 0.031 over the wideband frequency (2–18 GHz). Upon 20 years of aging, the VSWR increased to 7% and the radome-enclosed patch antenna gain decreased to 3%. The least variation in ε_r and δ (4% and 10%) and the reasonable retention of its gain value can be referred to as dielectric stability in high-speed communication/signal transmission applications.
- The SF/$E_{0.8}$ composite exhibited a good fiber/matrix adhesion and interface bonding. The amount and effect of moisture absorption in the (SF/$E_{0.8}$) reinforced PMC composite radome increased from 1.13% to 1.67% (at time = 0–25 years).
- With the increased accelerated aging time, the tensile strength of the SF/Ex composite decreased to 9.3% (147.81 MPa–133.94 MPa), compression strength to 6.4% (388.54 MPa–363.54 MPa), flexural strength to 14.5% (286.77 MPa–245.02 MPa), and ILSS to 22.3% (20.63 MPa–17.11 MPa), respectively.
- Accelerated environmental aging has deteriorated the fiber-matrix adhesion; however, the mechanical properties decreased gradually. Conclusively, as a function of aging time, the wave transparent composite was found with reliable dielectric properties, minimal moisture absorption, and good mechanical properties potentially suitable for high-speed communication/microelectronic applications.
- This work can be extended to develop a constitutive model to relate and optimize the dynamic changes which can affect the reliable performance of reinforced wave transparent composite radomes.

6 Future scope

For future work, it is recommended to include multiple stress factors (ultraviolet light, humidity cycling, corrosive environments, and dynamic aging) to validate/improve these findings. Applying wave-transparent surface coatings on the silica fiber/epoxy composite to reduce its environmental aging. In addition, the reliability study under dynamic stresses can be another interesting aspect for the future.

Data availability statement

The original contributions presented in the study are included in the article/Supplementary Material; further inquiries can be directed to the corresponding author.

Author contributions

IH: conceptualization, data curation, formal analysis, funding acquisition, investigation, methodology, software, writing–original draft, and writing–review and editing. IG: funding acquisition, investigation, methodology, project administration, resources, supervision, validation, visualization, writing–original draft, and writing–review and editing. SA: conceptualization, formal analysis, funding acquisition, investigation, project administration, software, writing–original draft, and writing–review and editing. MF: data curation, funding acquisition,

methodology, resources, supervision, visualization, writing–original draft, and writing–review and editing. MK: conceptualization, data curation, funding acquisition, investigation, project administration, supervision, writing–original draft, and writing–review and editing. SJ: conceptualization, data curation, formal analysis, funding acquisition, software, supervision, validation, visualization, writing–original draft, and writing–review and editing. D-WJ: data curation, formal analysis, funding acquisition, methodology, project administration, resources, supervision, validation, visualization, writing–original draft, and writing–review and editing.

Funding

The authors declare that financial support was received for the research, authorship, and/or publication of this article. This research was funded by the Brain Pool program of the Ministry of Science and by ICT through the National Research Foundation of Korea (RS-2023-00218940). This work was supported by the Deanship of Scientific Research, Vice Presidency for Graduate Studies and Scientific Research, King Faisal University, Saudi Arabia (Grant No. KFU241228).

Conflict of interest

The authors declare that the research was conducted in the absence of any commercial or financial relationships that could be construed as a potential conflict of interest.

Publisher's note

References

Adekomaya, O., Adediran, A., and Adama, K. (2018). Characterization and morphological properties of glass fiber reinforced epoxy composites fabricated under varying degrees of hand lay-up techniques. *J. Appl. Sci. Environ. Manag.* 22 (1), 110–114. doi:10.4314/jasem.v22i1.20

Ahmad, A., Khan, M. A., Akram, S., Faraz, M. I., Jaffery, S. H. I., Iqbal, T., et al. (2024). Achieving sustainable machining of titanium grade 3 alloy through optimization using grey relational analysis (GRA). *Results Eng.* 23, 102355. doi:10.1016/j.rineng.2024.102355

Amirapu, S. L., Nelapati, G. S., Yalamanchili, H., Badgayan, N. D., and Sahu, S. K. (2022). HDPE based polymeric nanodiamond nanocomposite for total knee arthoplasty: a finite element based approach. *Mater. Today Proc.* 56, 1622–1628. doi:10.1016/j.matpr.2022.03.290

Bilaç, O., and Duran, C. (2023). Mechanical, thermal, and dielectric properties of glass mullite composites for low-temperature cofired ceramic and radome applications. *Int. J. Appl. Ceram. Technol.* 20 (5), 3287–3296. doi:10.1111/ijac.14437

Boukhoulda, B., Adda-Bedia, E., and Madani, K. (2006). The effect of fiber orientation angle in composite materials on moisture absorption and material degradation after hygrothermal ageing. *Compos. Struct.* 74 (4), 406–418. doi:10.1016/j.compstruct.2005.04.032

Cecen, V., Seki, Y., Sarikanat, M., and Tavman, I. H. (2008). FTIR and SEM analysis of polyester-and epoxy-based composites manufactured by VARTM process. *J. Appl. Polym. Sci.* 108 (4), 2163–2170. doi:10.1002/app.27857

Champa-Bujaico, E., Díez-Pascual, A. M., Redondo, A. L., and Garcia-Diaz, P. (2024). Optimization of mechanical properties of multiscale hybrid polymer nanocomposites: a combination of experimental and machine learning techniques. *Compos. Part B Eng.* 269, 111099. doi:10.1016/j.compositesb.2023.111099

Chen, F., Xiao, H., Peng, Z. Q., Zhang, Z. P., Rong, M. Z., and Zhang, M. Q. (2021). Thermally conductive glass fiber reinforced epoxy composites with intrinsic self-healing capability. *Adv. Compos. Hybrid Mater.* 4, 1048–1058. doi:10.1007/s42114-021-00303-3

Choi, I., Kim, J. G., Seo, I. S., and Lee, D. G. (2012). Design of the hybrid composite face with electromagnetic wave transmission characteristics of low-observable radomes. *Compos. Struct.* 94 (11), 3394–3400. doi:10.1016/j.compstruct.2012.05.017

Clarricoats, P., Parini, C., and Rizk, M. (1982). "Performance of radome-covered reflector antennas," in *Iee proc. H microw. Opt. Antennas UK., IEE proceedings H (microwaves, optics and antennas)* (England: IET), 129, 153–160. doi:10.1049/ip-h-1.1982.0031

Cormier, L., and Joncas, S. (2010). "Effects of cold temperature, moisture and freeze-thaw cycles on the mechanical properties of unidirectional glass fiber-epoxy composites," in *51st AIAA/ASME/ASCE/AHS/ASC structures, structural dynamics, and materials conference 18th AIAA/ASME/AHS adaptive structures conference 12th*, 2823.

Deng, J., Song, Y., Lan, Z., Xu, Z., Chen, Y., Yang, B., et al. (2022). The surface modification effect on the interfacial properties of glass fiber-reinforced epoxy: a molecular dynamics study. *Nanotechnol. Rev.* 11 (1), 1143–1157. doi:10.1515/ntrev-2022-0068

Denis, L., Grzeskowiak, H., Trias, D., and Delaux, D. (2017). "Accelerated life testing," in *Reliability of high-power mechatronic systems 2* (Elsevier), 1–56.

Fu, X., Guo, Y., Du, Q., Guan, L., and He, S. (2019). Improved dielectric stability of epoxy composites with ultralow boron nitride loading. *RSC Adv.* 9 (8), 4344–4350. doi:10.1039/c8ra10211b

Fujimoto, D., Mizuno, Y., Takano, N., Sase, S., Negishi, H., and Sugimura, T. (2002). "Low-transmission-loss modified cyanate ester materials for high-frequency applications," in *2nd international IEEE conference on polymers and adhesives in microelectronics and photonics. POLYTRONIC 2002. Conference proceedings (cat. No. 02EX599)* (IEEE), 114–119.

Gu, J., Tang, Y., Kong, J., and Dang, J. (2024). *Polymer matrix wave-transparent composites: materials, properties, and applications*. John Wiley and Sons.

Ha, T. D., Zhu, L., Alsaab, N., Chen, P.-Y., and Guo, J. L. (2022). Optically transparent metasurface radome for rcs reduction and gain enhancement of multifunctional antennas. *IEEE Trans. Antennas Propag.* 71 (1), 67–77. doi:10.1109/tap.2022.3215247

Haider, I., Gul, I. H., Faraz, M. I., Aziz, S., Jaffery, S. H. I., Khan, M. A., et al. (2023a). Investigation of dielectric, mechanical, and thermal properties of epoxy composites embedded with quartz fibers. *Polymers* 15 (20), 4133. doi:10.3390/polym15204133

Haider, I., Gul, I. H., Umer, M. A., and Baig, M. M. (2023b). A low-cost silica fiber/epoxy composite with excellent dielectric properties, and good mechanical and thermal stability. *Materials* 16 (23), 7410. doi:10.3390/ma16237410

Hallberg, Ö., and Peck, D. S. (1991). Recent humidity accelerations, a base for testing standards. *Qual. Reliab. Eng. Int.* 7 (3), 169–180. doi:10.1002/qre.4680070308

Hong, S., Lee, C. S., Lee, M. H., Lee, Y., Ma, K. Y., Kim, G., et al. (2020). Ultralow-dielectric-constant amorphous boron nitride. *Nature* 582 (7813), 511–514. doi:10.1038/s41586-020-2375-9

Islam, M. Z., Fu, Y., Deb, H., Hasan, M. K., Dong, Y., and Shi, S. (2023). Polymer-based low dielectric constant and loss materials for high-speed communication network: dielectric constants and challenges. *Eur. Polym. J.* 200, 112543. doi:10.1016/j.eurpolymj.2023.112543

Jawaid, M., Meng, J., Wang, Y., and Kenawy, E.-R. (2016). A review on artificial aging behaviors of fiber reinforced polymer-matrix composites. *MATEC Web Conf.* 67, 06041. doi:10.1051/matecconf/20166706041

Karger-Kocsis, J., Mahmood, H., and Pegoretti, A. (2015). Recent advances in fiber/matrix interphase engineering for polymer composites. *Prog. Mater. Sci.* 73, 1–43. doi:10.1016/j.pmatsci.2015.02.003

Khan, M. A., Jaffery, S. H. I., and Khan, M. (2023b). Assessment of sustainability of machining Ti-6Al-4V under cryogenic condition using energy map approach. *Eng. Sci. Technol. Int. J.* 41, 101357. doi:10.1016/j.jestch.2023.101357

Khan, M. A., Jaffery, S. H. I., Khan, M., and Alruqi, M. (2023a). Machinability analysis of Ti-6Al-4V under cryogenic condition. *J. Mater. Res. Technol.* 25, 2204–2226. doi:10.1016/j.jmrt.2023.06.022

Khan, M. A., Sha, A., Yusuf, A., and Nisar, S. (2022). *Surface analysis of conversion coating of ASTM A 516*.

Khan, M. A., Shah, A., Jaffery, S. H. I., Khan, M., and Khan, A. R. (2019). "Analysis of surface treatment of ASTM A516 Grade 70 using Salt spray method," in *IOP conf. Ser, mater. Sci. Eng., IOP conference series: materials science and engineering* (London: IOP Publishing), 689, 012008. doi:10.1088/1757-899x/689/1/012008

Khattak, A., Amin, M., Iqbal, M., and Abbas, N. (2018). Life estimation and analysis of dielectric strength, hydrocarbon backbone and oxidation of high voltage multi stressed EPDM composites. *Mater. Res. Express* 5 (2), 025003. doi:10.1088/2053-1591/aaa82b

Kozakoff, D. J. (2010). *Analysis of radome-enclosed antennas*. Switzerland: Artech House.

Kumar Sahu, S., Dhar Badgayan, N., Samanta, S., and Rama Sreekanth, P. S. (2018). "Dynamic mechanical thermal analysis of high density polyethylene reinforced with nanodiamond, carbon nanotube and graphite nanoplatelet," in *Materials science forum* (Trans Tech Publ), 917, 27–31. 10.4028/www.scientific.net/MSF.917.27.

Kumosa, L., Benedikt, B., Armentrout, D., and Kumosa, M. (2004). Moisture absorption properties of unidirectional glass/polymer composites used in composite (non-ceramic) insulators. *Compos. Part A Appl. Sci. Manuf.* 35 (9), 1049–1063. doi:10.1016/j.compositesa.2004.03.008

Lasenko, I., Sanchaniya, J. V., Kanukuntla, S. P., Ladani, Y., Viluma-Gudmona, A., Kononova, O., et al. (2023). The mechanical properties of nanocomposites reinforced with PA6 electrospun nanofibers. *Polymers* 15 (3), 673. doi:10.3390/polym15030673

Li, C., Nie, Y., Zhan, H., Bai, J., Liu, T., and Gu, Y. (2022). Mechanical properties of polymer nanocomposites with randomly dispersed and cross-linked two-dimensional diamond. *Compos. Sci. Technol.* 230, 109722. doi:10.1016/j.compscitech.2022.109722

Li, H., Xiong, Z., Hao, W., and Yan, F. (2019). "Design and realization of a high transmission X-band radome for low-speed flight platform," in *2019 IEEE 2nd international conference on electronics technology (ICET)* (IEEE), 269–272.

Liu, P., Jin, Z., Li, Y., Chen, Z., Luo, Z., Liu, S., et al. (2023). Lifetime prediction and aging mechanism of glass fiber-reinforced acrylate–styrene–acrylonitrile/polycarbonate composite under long-term thermal and oxidative conditions. *J. Therm. Analysis Calorim.* 149, 2075–2085. doi:10.1007/s10973-023-12793-y

Mansouri, L., Djebbar, A., Khatir, S., and Abdel Wahab, M. (2019). Effect of hygrothermal aging in distilled and saline water on the mechanical behaviour of mixed short fibre/woven composites. *Compos. Struct.* 207, 816–825. doi:10.1016/j.compstruct.2018.09.067

Maxwell, A., Broughton, W., Dean, G., and Sims, G. (2005). *Review of accelerated ageing methods and lifetime prediction techniques for polymeric materials*.

McKenna, G. B. (2011). "Physical aging in glasses and composites," in *Long-term durability of polymeric matrix composites* (Springer), 237–309.

McKenna, G. B. (2012). *Physical aging in glasses and composites*, 237–309.

Muneer Ahmed, Z., Nasir, M. A., Iqbal, Z., and Aamir, M. T. (2024). Experimental investigation and simulation of electro-mechanical behaviour of hybrid sandwich composite radomes for aerospace applications. *Mech. Adv. Compos. Struct.* 11 (2), 401–412.

Nair, R. U., and Jha, R. M. (2009). Electromagnetic performance analysis of a novel monolithic radome for airborne applications. *IEEE Trans. antennas Propag.* 57 (11), 3664–3668. doi:10.1109/tap.2009.2026595

Nelo, M., Liimatainen, H., Väätäjä, M., Ukkola, J., Juuti, J., and Jantunen, H. (2019). Solid air—low temperature manufacturing of ultra-low permittivity composite materials for future telecommunication systems. *Front. Mater.* 6, 94. doi:10.3389/fmats.2019.00094

Nivedhitha, D. M., and Jeyanthi, S. (2023). Polyvinylidene fluoride—an advanced smart polymer for electromagnetic interference shielding applications—a novel review. *Polym. Adv. Technol.* 34 (6), 1781–1806. doi:10.1002/pat.6015

Nivedhitha, D. M., Jeyanthi, S., Rajamanickam, S. K., Balajivasan, R. J., R, H., Thiagamani, S. M. K., et al. (2023). Biopolymer-coated composites for enhanced dielectric and electromagnetic interference shielding applications-a green initiative. *Mater. Res. Express* 10 (10), 105013. doi:10.1088/2053-1591/ad0441

Panaitescu, I., Koch, T., and Archodoulaki, V.-M. (2019). Accelerated aging of a glass fiber/polyurethane composite for automotive applications. *Polym. Test.* 74, 245–256. doi:10.1016/j.polymertesting.2019.01.008

Park, S. Y., Choi, W. J., Choi, C. H., and Choi, H. S. (2019). An experimental study into aging unidirectional carbon fiber epoxy composite under thermal cycling and moisture absorption. *Compos. Struct.* 207, 81–92. doi:10.1016/j.compstruct.2018.08.069

Pradhan, S., Sahu, S. K., Pramanik, J., and Badgayan, N. D. (2022). An insight into mechanical and thermal properties of shape memory polymer reinforced with nanofillers; a critical review. *Mater. Today Proc.* 50, 1107–1112. doi:10.1016/j.matpr.2021.07.504

Qamar, Z., Salazar-Cerreno, J. L., and Aboserwal, N. (2020). An ultra-wide band radome for high-performance and dual-polarized radar and communication systems. *IEEE Access* 8, 199369–199381. doi:10.1109/access.2020.3032881

Rafieipour, H., Setoodeh, A., and Kin-Tak Lau, A. (2021). Mechanical and electromagnetic behavior of fabricated hybrid composite sandwich radome with a new optimized frequency-selective surface. *Compos. Struct.* 273, 114256. doi:10.1016/j.compstruct.2021.114256

Rodriguez, L. A. (2017). *Environmental durability and degradation of fiber-reinforced bismaleimide/quartz composite for aircraft radome applications*. PhD thesis. University of Miami.

Saba, N., Jawaid, M., and Sultan, M. (2019). "An overview of mechanical and physical testing of composite materials," in *Mechanical and physical testing of biocomposites, fibre-reinforced composites and hybrid composites*, 1–12.

Sahu, S. K., and Sreekanth, P. R. (2022). Artificial neural network for prediction of mechanical properties of HDPE based nanodiamond nanocomposite. *Polymer* 46 (5), 614–620. doi:10.7317/pk.2022.46.5.614

Salazar-Cerreno, J. L., Jehangir, S. S., Segales, A., Aboserwal, N., and Qamar, Z. (2022). "An ultrawideband uav-based metrology platform for *in-situ* em testing of antennas, radars, and communication systems," in *2022 IEEE radar conference (RadarConf22)* (IEEE), 1–5.

Selzer, R., and Friedrich, K. (1997). Mechanical properties and failure behaviour of carbon fibre-reinforced polymer composites under the influence of moisture. *Compos. Part A Appl. Sci. Manuf.* 28 (6), 595–604. doi:10.1016/s1359-835x(96)00154-6

Siddique, M. Z., Faraz, M. I., Butt, S. I., Khan, R., Petru, J., Jaffery, S. H. I., et al. (2023). Parametric analysis of tool wear, surface roughness and energy consumption during turning of inconel 718 under dry, wet and MQL conditions. *Machines* 11 (11), 1008. doi:10.3390/machines11111008

Silva, M. A., da Fonseca, B. S., and Biscaia, H. (2014). On estimates of durability of FRP based on accelerated tests. *Compos. Struct.* 116, 377–387. doi:10.1016/j.compstruct.2014.05.022

Starkova, O., Gagani, A. I., Karl, C. W., Rocha, I. B., Burlakovs, J., and Krauklis, A. E. (2022). Modelling of environmental ageing of polymers and polymer composites—durability prediction methods. *Polymers* 14 (5), 907. doi:10.3390/polym14050907

Tang, L., Zhang, J., Tang, Y., Kong, J., Liu, T., and Gu, J. (2021). Polymer matrix wave-transparent composites: a review. *J. Mater. Sci. Technol.* 75, 225–251. doi:10.1016/j.jmst.2020.09.017

Wallenberger, F. (1999). "Structural silicate and silica glass fibers," in *Advanced inorganic fibers: process-structure-properties-applications* (Springer), 129–168.

Wang, X. Q., Jian, W., Buyukozturk, O., Leung, C. K., and Lau, D. (2021). Degradation of epoxy/glass interface in hygrothermal environment: an atomistic investigation. *Compos. Part B Eng.* 206, 108534. doi:10.1016/j.compositesb.2020.108534

Wang, Y., Nan, S., Niu, N., and Zhang, J. (2020). "Establishment of accelerated degradation model and life evaluation method for external coating of airborne radome under ozone," in *2020 11th international conference on prognostics and system health management (PHM-2020 jinan)* (IEEE), 192–197.

Xing, Z., Yang, F., Yang, J., and Zhu, X. (2023). Low-RCS Ka-band receiving and transmitting satellite communication antennas co-designed with high-performance absorbent frequency-selective radomes. *J. Electromagn. Waves Appl.* 37 (2), 190–206. doi:10.1080/09205071.2022.2118086

Zhou, L., Pei, Y., and Fang, D. (2015). Dual-band A-sandwich radome design for airborne applications. *IEEE Antennas Wirel. Propag. Lett.* 15, 218–221. doi:10.1109/lawp.2015.2438552

Zhou, X., Liu, X., Cui, Z., Gu, J., Lin, S., and Zhuang, Q. (2020). Design and development of HMS@ ZIF-8/fluorinated polybenzoxazole composite films with excellent low-k performance, mechanical properties and thermal stability. *J. Mater. Chem. C* 8 (22), 7476–7484. doi:10.1039/d0tc00124d